JOURNAL OF GUIDANCE, CONTROL, AND DYNAMICS
Vol. 34, No. 2, March–April 2011

Decentralized Geolocation and Bias Estimation for Uninhabited Aerial Vehicles with Articulating Cameras

William Whitacre* and Mark E. Campbell†
Cornell University, Ithaca, New York 14853

DOI: 10.2514/1.49059

The cooperative geolocation of a point of interest using multiple uninhabited aerial vehicles with articulating camera sensors is addressed, where there are non-zero-mean errors (biases) in the estimate of the uninhabited aerial vehicle state. The proposed approach is to use the onboard navigation solution in the estimator and, further, to consider biases across all uninhabited aerial vehicles and to jointly estimate both the biases and the unknown point-of-interest location. Furthermore, a decentralized solution is presented that uses marginalization of the biases, thus allowing the uninhabited aerial vehicles to share only information about the point of interest and model only their local biases. This decentralized approach saves significant computation and scales well with the number of uninhabited aerial vehicles. Real flight-test data and hardware-in-the-loop simulations are used to demonstrate the improvement in geolocation with bias estimation, as well as the effectiveness of the new decentralized point of interest and bias estimation algorithm, for both stationary and moving points of interest.

I. Introduction

UNINHABITED aerial vehicles (UAVs) are currently being developed and used for a wide variety of missions such as defense, search-and-rescue [1], and commercial applications [2]. A key technology in UAV systems being explored is tracking of a stationary or moving point of interest (POI) using visual cameras for payloads, termed *geolocation*. Off-the-shelf digital cameras, which have been developed by the electronics industry for the past decade for consumer usage, are now enabling very-low-cost UAV systems. Several groups have implemented gimballing camera systems on UAVs [3,4], including a few with target-tracking results [5,6]. The authors have developed and experimentally implemented a geolocation tracking algorithm for gimballing vision payloads on UAVs [7] using sigma-point filtering concepts; extensions to information filtering and sensor fusion across multiple UAVs have also been developed [8].

The geolocation system for a UAV requires the complex integration of several hardware components [camera, UAV, Global Positioning System (GPS), and attitude sensors] and software components (camera image processing, inner-loop and path-planning control, and estimation software) to develop accurate estimates of the object being tracked. In [7,8], the authors reduce the computation of geolocation by using the onboard navigation system, which integrates the UAV, GPS, and attitude sensors to give an estimate of the position and attitude of the UAV and measurements of the camera gimbal angles. Further, there is an implicit assumption that the navigation system output and camera gimbal measurements have consistent statistics with zero-mean errors. However, this assumption is not valid, as shown in [9], because both the output of the navigation system and the camera gimbal measurements have non-zero-mean errors (biases) that significantly degrade geolocation performance. Campbell and Wheeler [7] compensate for these biases with an additional algorithm that fuses a conservative uniform density model for the bias.

Biases have also been shown to be a problem for estimation in other works. In one of the first treatments, Friedland [10] showed that biases could be estimated efficiently in a linear system by partitioning the state. More recently in [11,12], bias estimation in a radar tracking context with multiple targets was addressed. Bias estimation was further considered in [13,14], where multiple sensors were used to track multiple targets in a centralized formulation. Bias estimation has also been considered in a least-squares estimation context by Dogancay [15].

This paper proposes to jointly estimate the sensor biases and the unknown POI state in a decentralized manner, while using the solution from the onboard navigation system to save significant computation. Uniquely, the joint estimation problem is solved for multiple UAVs cooperating in a decentralized fashion, such that the UAVs share information on the POI state and model only their local biases. This decentralized formulation saves computation as well as communication, while giving geolocation accuracy that is comparable with the centralized case. Further, this decentralized approach fits nicely into the decentralized data fusion paradigm [16,17] and allows for effective cooperation not only among UAVs with potentially different biases, but among different sensors altogether. A numerical observability analysis procedure is also developed and applied, which gives a meaningful measure of the degree of observability and also gives insight into the effects of UAV flight path on observability. The new decentralized approach is validated using both experimental flight data and high-fidelity hardware-in-the-loop simulations. Although multitarget tracking is not considered in this work, extensions based on [18] can be considered.

The paper is organized as follows. In Sec. II, the cooperative geolocation problem is solved with explicit white zero-mean Gaussian assumptions on the estimate error of the UAV state. In Sec. III, a more realistic model including biases in the estimate of the UAV state is proposed and the joint POI and bias estimation problem is formulated and solved in both centralized and decentralized fashions. Section IV develops a procedure for observability analysis of both biases and the POI state. In Sec. V both experimental and simulated flight data for ScanEagle UAVs are used to evaluate the performance of the new decentralized approach compared with the centralized approach (baseline) for both stationary and moving POI.

II. Cooperative Geolocation

Geolocation is the process of using sensor data to develop statistical estimates of a POI on the ground. For the application of a vision sensor on a UAV, the UAV, based on its position and orientation, points the camera (through a gimballing payload mount

Presented as Paper 2009-6220 at the Guidance, Navigation, and Control Conference, Chicago, IL, 10–13 August 2009; received 26 January 2010; revision received 1 August 2010; accepted for publication 4 August 2010.

*Graduate Research Associate.
†Professor. Associate Fellow AIAA.

inside the UAV) at the POI on the ground. While the aircraft is moving (navigation and attitude) and the POI is potentially moving, the camera gimbals must adjust their angles to point at the POI. This application requires the camera to remain directed at the POI such that the POI always remains within the field of view of the camera. The objective of geolocation is then to estimate the position (2-D or 3-D) of the POI from the aircraft, gimbal, and camera measurements. Complicating this problem are uncertainties in the aircraft position and orientation, gimbal angles, camera specifications and measurements, and disturbances such as turbulence and engine vibrations.

The most accurate estimator tightly couples the UAV navigation (NAV), attitude (ATT), camera gimbal (GIM), and POI states in a single estimator, which requires full UAV and gimbal models, and a model for the POI. However, this estimator requires very high computation, memory, and communication in the case of multiple UAVs. Fortunately, most UAVs use a navigation system with estimators that provide statistics (estimates and covariances) for both the ATT and NAV states. In addition, the GIM states can be directly measured. Therefore, a geolocation estimator can be developed that estimates the POI state only, thus saving computation and memory.

A square-root sigma-point filter for geolocation, which uses the output statistics of the onboard navigation system of the UAVs to reduce computation, is described in [7]. A square-root sigma-point information filter is developed in [8] to facilitate cooperative tracking of POI using multiple UAVs. In both cases, to develop the POI estimate, there is an implied assumption that the estimates of the NAV and ATT states, as well as the measurements of the GIM states, have zero-mean errors. An extended information filter [19] (EIF) is developed here, which uses the navigation system to solve the cooperative geolocation problem and makes explicit the assumptions about the estimates of the UAV state. Note that an EIF is used here and presented in general terms to make the development of the decentralized bias estimation approaches in Sec. III clear. However, other filtering techniques could also be used.

For this section, define the state to be estimated, $\mathbf{x}_k$, to be the state of the POI, $\mathbf{x}_{k,\mathrm{POI}}$, with discrete-time dynamics governed by

$$\mathbf{x}_{k+1} = \mathbf{f}(\mathbf{x}_k, \mathbf{w}_k) = \mathbf{f}_{\mathrm{POI}}(\mathbf{x}_{k,\mathrm{POI}}, \mathbf{w}_{k,\mathrm{POI}}) \tag{1}$$

where the disturbance $\mathbf{w}_k = \mathbf{w}_{k,\mathrm{POI}}$ is zero-mean white Gaussian noise with covariance $\mathbf{Q}_k = \mathbf{Q}_{k,\mathrm{POI}}$, and the subscript k denotes time step t_k. Note that a general state to be estimated, $\mathbf{x}_k$, is used so that the bias estimation approaches in Sec. III can be developed easily as extensions of the EIF presented here. Assume there are N UAVs with states $\boldsymbol{\psi}^j_{k+1}$, for $j = 1, \ldots, N$, composed of UAV position $\boldsymbol{\psi}^j_{k+1,\mathrm{NAV}}$, UAV attitude $\boldsymbol{\psi}^j_{k+1,\mathrm{ATT}}$, and camera attitude $\boldsymbol{\psi}^j_{k+1,\mathrm{GIM}}$ written in vector form as

$$\boldsymbol{\psi}^j_{k+1} = \begin{bmatrix} \boldsymbol{\psi}^j_{k+1,\mathrm{NAV}} \\ \boldsymbol{\psi}^j_{k+1,\mathrm{ATT}} \\ \boldsymbol{\psi}^j_{k+1,\mathrm{GIM}} \end{bmatrix} \tag{2}$$

The UAVs are further assumed to have an onboard navigation system and measurements of the camera gimbal angles, which give an estimate of the UAV state $\hat{\boldsymbol{\psi}}^j_{k+1}$. For clarity in the development of the EIF, a simple model is used here and is given by

$$\boldsymbol{\psi}^j_{k+1} = \hat{\boldsymbol{\psi}}^j_{k+1} + \boldsymbol{\eta}^j_{k+1} \tag{3}$$

where the UAV state estimate error, $\boldsymbol{\eta}^j_{k+1}$, is zero-mean, Gaussian, and white with covariance, ${}^{\eta}\mathbf{R}^j_{k+1}$. This model is known to be incorrect because the statistics are not white, but correlated through the navigation filter. Many times, the errors due to autocorrelation are small [20]. Biases may also exist, however, which can have a significant effect on accuracy [9]. The incorporation of biases in the UAV state estimate, the focus of this paper, is presented in Sec. III as an extension of the EIF algorithm presented here.

Measurements of the POI are made on each UAV using

$$\mathbf{z}^j_{k+1} = \mathbf{h}^j(\mathbf{x}_{k+1}, \boldsymbol{\eta}^j_{k+1}, \mathbf{v}^j_{k+1}) = \mathbf{h}_{\mathrm{SCR}}(\mathbf{x}_{k+1,\mathrm{POI}}, \hat{\boldsymbol{\psi}}^j_{k+1} + \boldsymbol{\eta}^j_{k+1}, \mathbf{v}^j_{k+1,\mathrm{SCR}}) \tag{4}$$

where the sensor noise $\mathbf{v}^j_{k+1}$ is zero-mean white Gaussian noise with covariance ${}^{v}\mathbf{R}^j_{k+1}$. The process noise, sensor noises, and navigation system noises ($\mathbf{w}_k$, $\mathbf{v}^j_{k+1}$, and $\boldsymbol{\eta}^j_{k+1}$, respectively) are assumed to be uncorrelated with each other. Note that the measurement function in Eq. (4) is a complicated nonlinear function of the POI state and the UAV state; a detailed development is given in [7] with a summary provided in the Appendix.

The cooperative geolocation problem can now be solved with an EIF as follows. The information matrix $\mathbf{Y}_k$ and information state $\mathbf{y}_k$ are defined based on the state estimate error covariance $\mathbf{P}_k$ and state estimate $\hat{\mathbf{x}}_k$ as

$$\mathbf{Y}_k = \mathbf{P}_k^{-1} \tag{5}$$

$$\mathbf{y}_k = \mathbf{Y}_k \cdot \hat{\mathbf{x}}_k \tag{6}$$

The EIF algorithm is written for N UAVs, as computed on a local UAV l, as a recursion of the following fivesteps:

Step 1 is time propagation:

$$\mathbf{Y}^-_{k+1} = (\mathbf{F}_k \mathbf{Y}_k^{-1} \mathbf{F}_k^T + \Gamma_k \mathbf{Q}_k \Gamma_k^T)^{-1} \tag{7}$$

$$\mathbf{y}^-_{k+1} = \mathbf{Y}^-_{k+1} \cdot \mathbf{f}[(\mathbf{Y}_k)^{-1}\mathbf{y}_k, \mathbf{0}] \tag{8}$$

where

$$\mathbf{F}_k = \nabla_{\mathbf{x}} \mathbf{f}[\mathbf{x}, \mathbf{w}]|_{\mathbf{x}=(\mathbf{Y}_k)^{-1}\mathbf{y}_k, \mathbf{w}=\mathbf{0}} \tag{9}$$

$$\Gamma_k = \nabla_{\mathbf{w}} \mathbf{f}[\mathbf{x}, \mathbf{w}]|_{\mathbf{x}=(\mathbf{Y}_k)^{-1}\mathbf{y}_k, \mathbf{w}=\mathbf{0}} \tag{10}$$

For step 2, compute the local information state and matrix updates:

$$\mathbf{i}^l_{k+1} = ({}^{\mathbf{x}}\mathbf{H}^l_{k+1})^T (\mathbf{R}^l_{k+1})^{-1} (\mathbf{z}^l_{k+1} - \mathbf{h}^l[(\mathbf{Y}^-_{k+1})^{-1}\mathbf{y}^-_{k+1}, \mathbf{0}, \mathbf{0}] + {}^{\mathbf{x}}\mathbf{H}^l_{k+1}(\mathbf{Y}^-_{k+1})^{-1}\mathbf{y}^-_{k+1}) \tag{11}$$

$$\mathbf{I}^l_{k+1} = ({}^{\mathbf{x}}\mathbf{H}^l_{k+1})^T (\mathbf{R}^l_{k+1})^{-1} ({}^{\mathbf{x}}\mathbf{H}^l_{k+1}) \tag{12}$$

where

$$\mathbf{R}^l_{k+1} = {}^{\mathbf{v}}\mathbf{H}^l_{k+1} {}^{\mathbf{v}}\mathbf{R}^l_{k+1} ({}^{\mathbf{v}}\mathbf{H}^l_{k+1})^T + {}^{\boldsymbol{\eta}}\mathbf{H}^l_{k+1} {}^{\boldsymbol{\eta}}\mathbf{R}^l_{k+1} ({}^{\boldsymbol{\eta}}\mathbf{H}^l_{k+1})^T \tag{13}$$

and

$${}^{\mathbf{x}}\mathbf{H}^l_{k+1} = \nabla_{\mathbf{x}} \mathbf{h}^l[\mathbf{x}, \boldsymbol{\eta}, \mathbf{v}]|_{\mathbf{x}=(\mathbf{Y}^-_{k+1})^{-1}\mathbf{y}^-_{k+1}, \boldsymbol{\eta}=\mathbf{0}, \mathbf{v}=\mathbf{0}} \tag{14}$$

$${}^{\mathbf{v}}\mathbf{H}^l_{k+1} = \nabla_{\mathbf{v}} \mathbf{h}^l[\mathbf{x}, \boldsymbol{\eta}, \mathbf{v}]|_{\mathbf{x}=(\mathbf{Y}^-_{k+1})^{-1}\mathbf{y}^-_{k+1}, \boldsymbol{\eta}=\mathbf{0}, \mathbf{v}=\mathbf{0}} \tag{15}$$

$${}^{\boldsymbol{\eta}}\mathbf{H}^l_{k+1} = \nabla_{\boldsymbol{\eta}} \mathbf{h}^l[\mathbf{x}, \boldsymbol{\eta}, \mathbf{v}]|_{\mathbf{x}=(\mathbf{Y}^-_{k+1})^{-1}\mathbf{y}^-_{k+1}, \boldsymbol{\eta}=\mathbf{0}, \mathbf{v}=\mathbf{0}} \tag{16}$$

For step 3, transmit local information updates $\mathbf{i}^l_{k+1}$ and $\mathbf{I}^l_{k+1}$ to all UAVs.

For step 4, receive information updates $\mathbf{i}^j_{k+1}$ and $\mathbf{I}^j_{k+1}$ from all UAVs, for $j = 1, \ldots, N$ and $j \neq l$.

For step 5, fuse local and received information updates:

$$\mathbf{Y}_{k+1} = \mathbf{Y}^-_{k+1} + \mathbf{I}^l_{k+1} + \sum_{j=1, j\neq l}^{N} \mathbf{I}^j_{k+1} \tag{17}$$

$$\mathbf{y}_{k+1} = \mathbf{y}^{-}_{k+1} + \mathbf{i}^{l}_{k+1} + \sum_{j=1, j\neq l}^{N} \mathbf{i}^{j}_{k+1} \tag{18}$$

The assumptions on the errors of the navigation system output (white zero-mean Gaussian) are necessary for the computation of the information state and matrix updates (step 2) and allow the uncertainty in both the vision system (${}^{\nu}\mathbf{R}^{l}_{k+1}$) and the navigation system (${}^{\eta}\mathbf{R}^{l}_{k+1}$) to be combined in Eq. (13) to compute the effective measurement noise covariance $\mathbf{R}^{l}_{k+1}$. Note that the superscript l is not included for the information matrix and state, since they are the same on all UAVs. If communication losses are present, causing differences among the UAVs, then the above algorithm can be extended using the predicted information approach developed in [21].

III. Geolocation with Bias Estimation

The assumption in Sec. II that the errors in the estimate of the UAV state are zero-mean, white, and Gaussian is not accurate in the practical case, for two reasons: correlated outputs of the navigation filter and biases in the outputs. Consider Fig. 1, which shows a series of sensed points of interest (SPOI), which is defined as the line-of-sight intersection of the camera with the ground as computed based on the estimates of the UAV state (NAV, ATT, and GIM). A total of 2000 SPOI are plotted for two orbits around a stationary POI from a flight test of the ScanEagle UAV on 18 March 2006 [9]. Figure 1 shows that the SPOI moves in a roughly circular pattern around the true POI location. The period of this oscillation corresponds directly to the UAVs orbit about the POI and is due to non-zero-mean errors (biases) in the UAV state estimate.

Sensor biases were shown in [7,9] to be a significant source of error for geolocation and were compensated for by augmenting the output of the estimator with additional uncertainty, based on empirical data. However, this did nothing to improve the estimate itself, but simply improved estimator consistency. The approach taken here is to explicitly model the sensor biases and jointly estimate both the sensor biases and the unknown POI location in a decentralized manner. The biases $\mathbf{b}^{j}_{k}$ are now modeled explicitly as part of the UAV navigation system output and camera gimbal measurement as

$$\boldsymbol{\psi}^{j}_{k} = \hat{\boldsymbol{\psi}}^{j}_{k} + \mathbf{b}^{j}_{k} + \boldsymbol{\eta}^{j}_{k} \tag{19}$$

where the model of the bias state $\mathbf{b}^{j}_{k}$ used here is

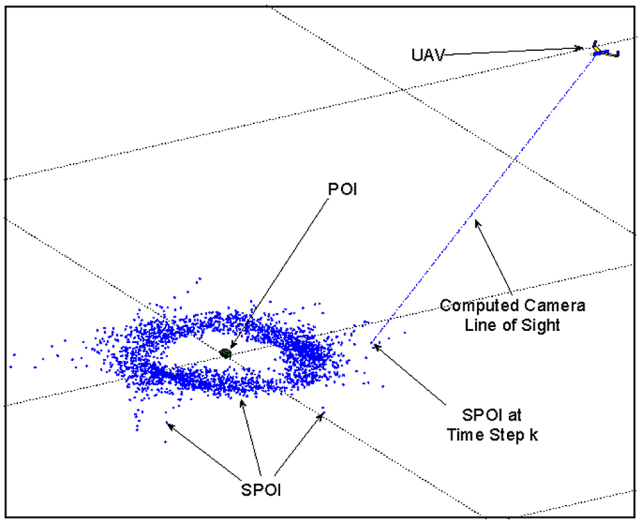

Fig. 1 Single UAV tracking a stationary POI. The dots are the computed camera line-of-sight intersections with the ground from two orbits of tracking.

$$\mathbf{b}^{j}_{k+1} = \mathbf{b}^{j}_{k} + \mathbf{w}_{k,\mathbf{b}^{j}} \tag{20}$$

Autocorrelation of the UAV state estimate error could be taken into account in the same way as the biases [22]: by adding autocorrelation states $\boldsymbol{\mu}^{j,m}_{k}$ in Eq. (19) as

$$\boldsymbol{\psi}^{j}_{k} = \hat{\boldsymbol{\psi}}^{j}_{k} + \mathbf{b}^{j}_{k} + \boldsymbol{\eta}^{j}_{k} + \boldsymbol{\mu}^{j,1}_{k} + \ldots + \boldsymbol{\mu}^{j,n_{\mu^j}}_{k} \tag{21}$$

where each of the autocorrelation terms correspond to a different frequency of autocorrelation. The autocorrelation terms can be modeled as

$$\boldsymbol{\mu}^{j,m}_{k+1} = a^{j,m}\boldsymbol{\mu}^{j,m}_{k} + \mathbf{w}_{k,\boldsymbol{\mu}_{j,m}} \tag{22}$$

where the parameter $a^{j,m}$ is chosen to capture the appropriate autocorrelation frequency. Although autocorrelations are not considered in this work, the approach presented here is suitable for autocorrelation errors in addition to bias errors.

A key point of the approach here is that the navigation system and camera gimbal measurements are used directly, while only the biases $\mathbf{b}^{j}$ are estimated, recursively, with the POI state $\mathbf{x}_{k,\mathrm{POI}}$. This uses the navigation system to save significant computation, while effectively improving the estimate of the UAV state and thus improving geolocation.

A. Centralized Approach

With the goal of estimating the POI state $\mathbf{x}_{\mathrm{POI}}$ and the biases $\mathbf{b}^{j}$ on each UAV, the obvious approach is to create a single estimator; this is termed the centralized solution. In the centralized solution, the state to be estimated, $\mathbf{x}_{k}$, is modified to include the state of the POI, $\mathbf{x}_{k,\mathrm{POI}}$, and the biases of each of the UAVs, $\mathbf{b}^{j}_{k}$, for $j = 1, \ldots, N$. The full state estimate and error covariance are now written as

$$\hat{\mathbf{x}}_{k} = \begin{bmatrix} \hat{\mathbf{x}}_{k,\mathrm{POI}} \\ \hat{\mathbf{b}}^{1}_{k} \\ \vdots \\ \hat{\mathbf{b}}^{N}_{k} \end{bmatrix}$$
$$\mathbf{P}_{k} = \begin{bmatrix} \mathbf{P}_{k,\mathrm{POI},\mathrm{POI}} & \mathbf{P}_{k,\mathrm{POI},\mathbf{b}^{1}} & \cdots & \mathbf{P}_{k,\mathrm{POI},\mathbf{b}^{N}} \\ \mathbf{P}_{k,\mathbf{b}^{1},\mathrm{POI}} & \mathbf{P}_{k,\mathbf{b}^{1},\mathbf{b}^{1}} & \cdots & \mathbf{P}_{k,\mathbf{b}^{1},\mathbf{b}^{N}} \\ \vdots & \vdots & \ddots & \vdots \\ \mathbf{P}_{k,\mathbf{b}^{N},\mathrm{POI}} & \mathbf{P}_{k,\mathbf{b}^{N},\mathbf{b}^{1}} & \cdots & \mathbf{P}_{k,\mathbf{b}^{N},\mathbf{b}^{N}} \end{bmatrix} \tag{23}$$

The EIF algorithm presented in Sec. II can now be applied by making changes to the dynamics model (1) and the measurement model (4). First, the dynamics model is augmented to include models of the bias states as

$$\mathbf{x}_{k+1} = \mathbf{f}(\mathbf{x}_{k}, \mathbf{w}_{k}) = \begin{bmatrix} \mathbf{f}_{\mathrm{POI}}(\mathbf{x}_{k,\mathrm{POI}}, \mathbf{w}_{k,\mathrm{POI}}) \\ \mathbf{b}^{1}_{k} + \mathbf{w}_{k,\mathbf{b}^{1}} \\ \vdots \\ \mathbf{b}^{N}_{k} + \mathbf{w}_{k,\mathbf{b}^{N}} \end{bmatrix} \tag{24}$$

and the process noise covariance $\mathbf{Q}_{k}$ includes the covariance for the process noise of the POI as well as the bias and is given by

$$\mathbf{Q}_{k} = \begin{bmatrix} \mathbf{Q}_{k,\mathrm{POI}} & \mathbf{0} & \cdots & \mathbf{0} \\ \mathbf{0} & \mathbf{Q}_{k,\mathbf{b}^{1}} & \ddots & \vdots \\ \vdots & \ddots & \ddots & \mathbf{0} \\ \mathbf{0} & \cdots & \mathbf{0} & \mathbf{Q}_{k,\mathbf{b}^{N}} \end{bmatrix} \tag{25}$$

Second, the measurement model must be modified to include the biases and is written for the jth UAV as

$$\mathbf{z}^{j}_{k+1} = \mathbf{h}^{j}(\mathbf{x}_{k+1}, \boldsymbol{\eta}^{j}_{k+1}, \mathbf{v}^{j}_{k+1}) = \mathbf{h}_{\mathrm{SCR}}(\mathbf{x}_{k+1,\mathrm{POI}}, \hat{\boldsymbol{\psi}}^{j}_{k+1} + \mathbf{b}^{j}_{k+1} + \boldsymbol{\eta}^{j}_{k+1}, \mathbf{v}^{j}_{k+1,\mathrm{SCR}}) \tag{26}$$

The EIF algorithm from Sec. II can now be applied with the new dynamics and measurement equations.

The augmentation of the POI state with the biases of each UAV in the centralized approach is statistically correct,[‡] but there are two significant problems with such a formulation. First, each UAV must model the dynamics and maintain estimates of the biases of all other UAVs [Eq. (24)]. This violates one of the basic concepts of decentralized data fusion [17] and hence is termed here as the centralized approach. Second, the size of the state to be estimated scales with the number of UAVs (N), and therefore the computation scales poorly with the number of UAVs. In fact, the information filter requires a matrix inverse to recover the state estimate and covariance, and this operation scales cubically with the size of the state. A decentralized approach is proposed in the next section, and the centralized solution is used in Sec. V to provide a benchmark for comparison.

B. Decentralized Approach

The decentralized approach developed here requires the UAVs to model only the POI and their own biases and to only share information related to the POI state. Thus, the decentralized approach scales well with the number of UAVs and requires less computation and communication than the centralized approach. In the decentralized approach, the state to be estimated on each UAV, $\mathbf{x}_k^j$, includes only the state of the POI, $\mathbf{x}_{k,\mathrm{POI}}$, and the local biases $\mathbf{b}_k^j$ and is written as

$$\mathbf{x}_k^j = \begin{bmatrix} \mathbf{x}_{k,\mathrm{POI}} \\ \mathbf{b}_k^j \end{bmatrix} \quad \text{for } j = 1, \ldots, N \tag{27}$$

Note that the superscript j is included as the state to be estimated is different on each UAV, and hence the estimates and covariances (information states and matrices) are different on each UAV. The state dynamics are modified to include only the POI and local biases as

$$\begin{aligned} \mathbf{x}_{k+1}^j &= \mathbf{f}(\mathbf{x}_k^j, \mathbf{w}_k^j) = \begin{bmatrix} \mathbf{f}_{\mathrm{POI}}(\mathbf{x}_{k,\mathrm{POI}}, \mathbf{w}_{k,\mathrm{POI}}) \\ \mathbf{b}_k^j + \mathbf{w}_{k,\mathbf{b}^j} \end{bmatrix}, \\ \mathbf{Q}_k^j &= \begin{bmatrix} \mathbf{Q}_{k,\mathrm{POI}} & \mathbf{0} \\ \mathbf{0} & \mathbf{Q}_{k,\mathbf{b}^j} \end{bmatrix} \end{aligned} \tag{28}$$

Note that the measurement [Eq. (26)] for each UAV remains the same, since it already contains only local biases.

In the decentralized formulation, the state estimate and error covariance are written as

$$\hat{\mathbf{x}}_k^j = \begin{bmatrix} \hat{\mathbf{x}}_{k,\mathrm{POI}}^j \\ \hat{\mathbf{b}}_k^j \end{bmatrix}, \qquad \mathbf{P}_k^j = \begin{bmatrix} \mathbf{P}_{k,\mathrm{POI,POI}}^j & \mathbf{P}_{k,\mathrm{POI},\mathbf{b}^j}^j \\ \mathbf{P}_{k,\mathbf{b}^j,\mathrm{POI}}^j & \mathbf{P}_{k,\mathbf{b}^j,\mathbf{b}^j}^j \end{bmatrix} \tag{29}$$

and the usual conversion between state and information space applies:

$$\mathbf{Y}_k^j = (\mathbf{P}_k^j)^{-1} \qquad \mathbf{y}_k^j = \mathbf{Y}_k^j \hat{\mathbf{x}}_k^j \tag{30}$$

The information state and matrix are propagated forward in time, using Eqs. (7) and (8) to get $\mathbf{Y}_{k+1}^{j-}$ and $\mathbf{y}_{k+1}^{j-}$. The local information state and matrix updates are computed using Eqs. (11) and (12) to get

$$\mathbf{I}_{k+1}^j = \begin{bmatrix} \mathbf{I}_{k,\mathrm{POI,POI}} & \mathbf{I}_{k,\mathrm{POI},\mathbf{b}^j} \\ \mathbf{I}_{k,\mathbf{b}^j,\mathrm{POI}} & \mathbf{I}_{k,\mathbf{b}^j,\mathbf{b}^j} \end{bmatrix}, \qquad \mathbf{i}_{k+1}^j = \begin{bmatrix} \mathbf{i}_{k,\mathrm{POI}} \\ \mathbf{i}_{k,\mathbf{b}^j} \end{bmatrix} \tag{31}$$

With N decentralized estimators of the form described in Eq. (29), it is noted that only the POI state is common across each of the estimators, and thus it is desired to share only information related to the POI states. However, communication and fusion of only the POI state portion of the information updates, $\mathbf{I}_{k,\mathrm{POI,POI}}$ and $\mathbf{i}_{k,\mathrm{POI}}$, is not statistically correct, unfortunately. The offdiagonal portion of the information matrix updates, $\mathbf{I}_{k,\mathrm{POI},\mathbf{b}^j}$, actually serves to reduce the information about the target because of the coupling with the uncertainty in the bias states. It is proposed to account for this coupling using two marginalization steps before communication and fusion.

The process of computing and fusing the marginalized information updates is written for a local UAV l as follows. The first step is to fuse the local information updates as

$$\mathbf{Y}_{k+1}^l = \mathbf{Y}_{k+1}^{l-} + \mathbf{I}_{k+1}^l \tag{32}$$

$$\mathbf{y}_{k+1}^l = \mathbf{y}_{k+1}^{l-} + \mathbf{i}_{k+1}^l \tag{33}$$

which includes information about the local POI and bias estimates to be incorporated [Eq. (31)].

The second step is to compute two marginalizations in order to prepare the information to be communicated to the other UAVs. Marginalization of the *predicted* bias states begins by converting the predicted information state and matrix back to state space as

$$\begin{aligned} \mathbf{P}_{k+1}^{l-} &= (\mathbf{Y}_{k+1}^{l-})^{-1} = \begin{bmatrix} \mathbf{P}_{k,\mathrm{POI,POI}}^{l-} & \mathbf{P}_{k,\mathrm{POI},\mathbf{b}^l}^{l-} \\ \mathbf{P}_{k,\mathbf{b}^l,\mathrm{POI}}^{l-} & \mathbf{P}_{k,\mathbf{b}^l,\mathbf{b}^l}^{l-} \end{bmatrix}, \\ \hat{\mathbf{x}}_{k+1}^{l-} &= \mathbf{P}_{k+1}^{l-} \mathbf{y}_{k+1}^{l-} = \begin{bmatrix} \hat{\mathbf{x}}_{k,\mathrm{POI}}^{l-} \\ \hat{\mathbf{b}}_k^{l-} \end{bmatrix} \end{aligned} \tag{34}$$

Then in the state space, the bias states are marginalized out by simply removing the corresponding rows and columns of the predicted covariance and state estimate, since the joint POI and bias state is multivariate Gaussian. The marginalized M covariance and state estimate are given as

$$\mathbf{P}_{k+1,M}^{l-} = \mathbf{P}_{k+1,\mathrm{POI,POI}}^{l-}, \qquad \hat{\mathbf{x}}_{k+1,M}^{l-} = \hat{\mathbf{x}}_{k+1,\mathrm{POI}}^{l-} \tag{35}$$

The marginalized estimate and covariance are then converted back to information space as

$$\mathbf{Y}_{k+1,M}^{l-} = (\mathbf{P}_{k+1,M}^{l-})^{-1} \qquad \mathbf{y}_{k+1,M}^{l-} = \mathbf{Y}_{k+1,M}^{l-} \hat{\mathbf{x}}_{k+1,M}^{l-} \tag{36}$$

This marginalization process is then repeated for the *updated* information matrix $\mathbf{Y}_{k+1}^l$ and state $\mathbf{y}_{k+1}^l$ to get $\mathbf{Y}_{k+1,M}^l$ and $\mathbf{y}_{k+1,M}^l$.

The third step is to compute the marginalized information state and matrix updates as

$$\mathbf{I}_{k+1,M}^l = \mathbf{Y}_{k+1,M}^l - \mathbf{Y}_{k+1,M}^{l-} \tag{37}$$

$$\mathbf{i}_{k+1,M}^l = \mathbf{y}_{k+1,M}^l - \mathbf{y}_{k+1,M}^{l-} \tag{38}$$

The final step is to communicate the local marginalized information matrix and state updates to the other UAVs. Locally, all received updates are then fused as

$$\mathbf{Y}_{k+1}^l \Leftarrow \mathbf{Y}_{k+1}^l + \sum_{j=1, j\neq l}^{N} \begin{bmatrix} \mathbf{I}_{k+1,M}^j & \mathbf{0}_{n_{\mathrm{POI}}, n_{\mathbf{b}^l}} \\ \mathbf{0}_{n_{\mathbf{b}^l}, n_{\mathrm{POI}}} & \mathbf{0}_{n_{\mathbf{b}^l}, n_{\mathbf{b}^l}} \end{bmatrix} \tag{39}$$

$$\mathbf{y}_{k+1}^l \Leftarrow \mathbf{y}_{k+1}^l + \sum_{j=1, j\neq l}^{N} \begin{bmatrix} \mathbf{i}_{k+1,M}^j \\ \mathbf{0}_{n_{\mathbf{b}^l}, 1} \end{bmatrix} \tag{40}$$

where $\mathbf{0}_{m,n}$ is an $m \times n$ matrix of zeros, n_{POI} is the dimension of the POI state, and $n_{\mathbf{b}^l}$ is the dimension of the biases being estimated on UAV l.

The marginalization steps accomplish two objectives:

1) The marginalized information updates are for the POI state only. This means that UAVs with different types of biases or even different types of sensors can effectively cooperate in geolocation. Further, no knowledge of the biases, or even of the measurement models of the other UAVs, is required.

[‡]Statistical correctness is used here to mean that the statistics of each of the random variables are accurately captured with a filter that linearizes the system dynamics and output.

2) The uncertainty in the bias states is used to reduce the information update on the POI, to account for uncertainty in the bias estimates. This improves estimator consistency over no bias estimation, while still improving geolocation accuracy with local bias estimates.

However, marginalization causes some information to be lost. Specifically, the cross correlation among the biases is no longer maintained: i.e., $\mathbf{P}_{\mathbf{b}^j,\mathbf{b}^l} \equiv \mathbf{0}$ in the decentralized formulation. Though not statistically correct, as long as the cross correlation is small, there is only a small reduction in geolocation accuracy over the centralized solution. This small loss of accuracy in geolocation is traded for significant gains in scalability, computation, and communication. Further, this decentralized solution fits nicely into the decentralized data fusion paradigm.

IV. Observability Procedure

In Sec. III, the POI and bias estimation problem is formulated with the potential for biases in the UAV position ($\mathbf{b}_{k,\mathrm{NAV}}$), UAV attitude ($\mathbf{b}_{k,\mathrm{ATT}}$), and camera attitude ($\mathbf{b}_{k,\mathrm{GIM}}$). This section develops a procedure for evaluating the observability of both the POI and bias states. Because of the nonlinear measurement function for a camera sensor, shown in the Appendix, this is a nonlinear observability problem. Therefore, a numerical procedure following [23,24] is developed that uses the inverse of the observability gramian.

The observability gramian at time step K is given by

$$\mathcal{Q}_K = \mathcal{O}_K^T \mathcal{O}_K \tag{41}$$

where $\mathcal{O}_K$ is the observability matrix at time step K and is given by

$$\mathcal{O}_K = \begin{bmatrix} {}^{\mathbf{x}}\mathbf{H}_1 \\ {}^{\mathbf{x}}\mathbf{H}_2\mathbf{F}_1 \\ \vdots \\ {}^{\mathbf{x}}\mathbf{H}_K\mathbf{F}_{K-1}\cdots\mathbf{F}_1 \end{bmatrix} \tag{42}$$

with ${}^{\mathbf{x}}\mathbf{H}$ defined in Eq. (14) and $\mathbf{F}$ defined in Eq. (9). Note that only one UAV is considered here, and therefore the superscripts denoting the UAV are not used in this section. Extensions of the observability analysis to multiple UAVs is straight forward.

Observability requires $\mathcal{Q}$ or, equivalently, $\mathcal{O}$ be full rank. A scaled version of the observability gramian, which gives physical insight into the degree of observability, is used here and defined as

$$\bar{\mathcal{Q}}_K = \mathcal{O}_K^T \mathcal{R}_K^{-1} \mathcal{O}_K \tag{43}$$

where $\mathcal{R}_K$ is used to scale the observability gramian based on the effective sensor noise covariance:

$$\mathcal{R}_K = \begin{bmatrix} \mathbf{R}_1 & & \mathbf{0} \\ & \ddots & \\ \mathbf{0} & & \mathbf{R}_K \end{bmatrix} \tag{44}$$

where it is noted that $\mathcal{R}_K$ is full rank.

Three important observations are made regarding this scaled observability gramian.

1) Since observability is determined by the rank of $\mathcal{Q}_K$, observability can also be inferred from $\bar{\mathcal{Q}}_K$, since

$$\mathrm{rank}\,(\mathcal{Q}_K) = \mathrm{rank}(\bar{\mathcal{Q}}_K) \tag{45}$$

2) $\bar{\mathcal{Q}}_K$ has a physically meaningful interpretation. In the case of no process noise, i.e., $\mathbf{Q} = \mathbf{0}$, $\bar{\mathcal{Q}}_K^{-1}$ is the error covariance at time step K if one starts with a diffuse prior: $\mathbf{Y}_0 = \mathbf{0}$.

3) If the POI is stationary, $\mathbf{F}_k = \mathcal{I}$, then $\bar{\mathcal{Q}}_K$ can be computed recursively by summing the information matrix updates $\mathbf{I}_k$ in Eq. (12) as

$$\bar{\mathcal{Q}}_K = \sum_{k=1}^{K} \mathbf{I}_k \tag{46}$$

The process for determining observability is summarized as follows. First, define the state to be considered: $\mathbf{x}^*$. For example, the most general joint POI and bias state is $\mathbf{x}^* = [\mathbf{x}_{\mathrm{POI}}^T, \ \mathbf{b}_{\mathrm{NAV}}^T, \ \mathbf{b}_{\mathrm{ATT}}^T, \ \mathbf{b}_{\mathrm{GIM}}^T]^T$. Define a time step of interest, such as $K = k_{\mathrm{orbit}}$, where k_{orbit} is the number of time steps for the UAV to make a single orbit about the POI. Then compute $\bar{\mathcal{Q}}_K$ using Eq. (43). Finally, check the rank of $\bar{\mathcal{Q}}_K$; the state $\mathbf{x}^*$ is then observable if and only if $\bar{\mathcal{Q}}_K$ is full rank. If $\bar{\mathcal{Q}}_K$ is full rank, then the degree of observability can be assessed by taking the inverse of $\bar{\mathcal{Q}}_K$ to get $\bar{\mathcal{P}}_K$. The matrix $\bar{\mathcal{P}}_K$ denotes the error covariance when starting with a diffuse prior and no process noise. Large values of the diagonal of $\bar{\mathcal{P}}_K$ indicate poor observability. Further, if some of the elements of the state $\mathbf{x}^*$ have comparable units, e.g., $\mathbf{b}_{\mathrm{ATT}}$ and $\mathbf{b}_{\mathrm{GIM}}$, then the modes and degree of observability can be determined by analyzing the eigenvalues Λ and eigenvectors V of the submatrix of $\bar{\mathcal{P}}_K$ corresponding to those states. Large elements of Λ indicate poor observability, and the corresponding eigenvector yields the related combination of the elements of $\mathbf{x}^*$.

V. Validation with Experimental and Simulated Flight Data

The decentralized bias estimation approach presented in Sec. III is evaluated and compared with the centralized solution using both experimental flight-test data and hardware-in-the-loop (HIL) simulations. Additionally, the procedure for observability analysis developed in Sec. IV is used to evaluate the observability of the POI and bias states. Note that due to International Traffic in Arms Regulations (ITAR) restrictions, all results are scaled to avoid showing absolute performance. However, since a consistent scaling is used for all results, all relative comparisons should be clear.

A. Experimental and Simulated Flight-Test Setup

Both experimental flight data and HIL simulations are used. Figure 2 shows the orbit configuration used for both the experimental and HIL tests, including relative phasing between the UAVs, β, and orbit offsets from the POI, Δ. The UAVs are shown as triangles and the POI is shown as a star.

Experimental flight data were collected during a cooperative UAV flight test on 16 March 2007 at the Boeing Boardman test range, which is classified as a military operations area. In this test, two UAVs orbited a stationary POI, with a POI-centered orbit, $\Delta = 0$, and an orbit radius of 500 m. For this test, a van was used as the POI and the true location was measured using a local GPS receiver. The experimental flight test is described in more detail in [25].

In addition to the experimental flight data, a series of high-fidelity HIL simulations were performed. The HIL simulations include realistic environmental effects such as wind, as well as the actual

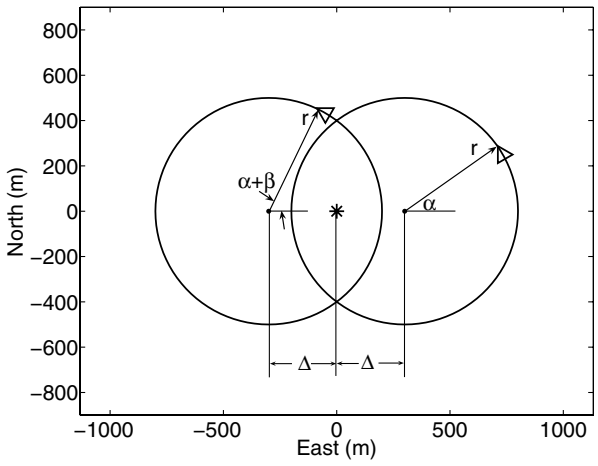

Fig. 2 Diagram illustrating the configuration (in projected 2-D) of two UAVs (triangle) orbiting above a POI (∗) performing geolocation. The orbits are parameterized by the relative phase β and orbit offset Δ.

Table 1 Test configurations for the HIL simulations

HIL test number	POI motion	Phase β, deg	Orbit offset Δ, m
1	Stationary	[0,30,...,180]	0
2	Stationary	150	[0,50,...,500]
3	Moving	[0,30,...,180]	0

onboard guidance software that coordinates the motion of the UAVs [26,27]. HIL simulations were performed to generate flight data for both stationary and moving POI. Tests were performed for a range of relative phase angles between the UAVs and offsets to their orbits from the POI. The HIL test configurations used are summarized in Table 1.

For each HIL test, bias errors were added to the UAV attitude and camera attitude. The values of the biases were chosen to be representative and are not shown, due to ITAR restrictions. The trajectory of the POI in the moving-POI case is based on a city driving model, which is characterized by frequent stops and 90° turns. The FlockGuidance software [26,27] is used to maintain the configuration, shown in Fig. 2, relative to the moving POI. For each test of a moving POI, a different POI trajectory is used, and constant bias errors are added to both the camera and UAV attitude estimates. Note that the bias errors are the same for each test, but they are different for each UAV.

B. Stationary-POI Results

Geolocation and bias estimation for a stationary POI are evaluated with both experimental flight-test data and HIL simulations. A stationary POI is modeled as

$$\mathbf{x}_{k+1,\mathrm{POI}} = \mathbf{x}_{k,\mathrm{POI}} + \mathbf{w}_{k,\mathrm{POI}} \tag{47}$$

where the state of the POI, $\mathbf{x}_{k,\mathrm{POI}}$, is the position in a local north–east–down (NED) frame. The process noise $\mathbf{w}_{k,\mathrm{POI}}$ is white Gaussian noise with a relatively small covariance, $\mathbf{Q}_{k,\mathrm{POI}} = 0.05 \cdot \mathcal{I}_{n_{\mathrm{POI}}}$ m/s, which is included to prevent premature convergence. The stationary-POI results are organized as follows. First, the case of a single UAV is considered, including an observability analysis and a geolocation error evaluation. Second, cooperative geolocation is evaluated using the experimental flight-test data, which includes two UAVs in circular orbits about a stationary POI.

1. Single UAV

First, consider the observability of the POI and bias states using a single UAV, a stationary POI, and a POI-centered orbit for the UAV. Observability is evaluated using the procedure developed in Sec. IV. The state $\mathbf{x}^*$ is defined to be the state of the POI and all possible biases:

$$\mathbf{x}^* = \begin{bmatrix} \mathbf{x}_{\mathrm{POI}} \\ \mathbf{b}_{\mathrm{NAV}} \\ \mathbf{b}_{\mathrm{ATT}} \\ \mathbf{b}_{\mathrm{GIM}} \end{bmatrix} \tag{48}$$

where the dimension of $\mathbf{x}^*$ is 12. Further, define $K = k_{\mathrm{orbit}}$, where k_{orbit} is the number of time steps for the UAV to complete one orbit about the POI. Note that one orbit is used here, because the UAV continually repeats orbits about the POI. The observability of $\mathbf{x}^*$ is evaluated by computing $\bar{\mathcal{Q}}_K$ as in Eq. (43) and then computing the rank, giving, in this case,

$$\mathrm{rank}\,(\bar{\mathcal{Q}}_K) = 9 \tag{49}$$

which is a rank deficiency of 3. This indicates that not all states of $\mathbf{x}^*$ are observable.

Consider the effect of removing the UAV navigation bias from $\mathbf{x}^*$, i.e., redefining $\mathbf{x}^*$ to be

$$\mathbf{x}^* = \begin{bmatrix} \mathbf{x}_{\mathrm{POI}} \\ \mathbf{b}_{\mathrm{ATT}} \\ \mathbf{b}_{\mathrm{GIM}} \end{bmatrix} \tag{50}$$

where the dimension of $\mathbf{x}^*$ is now 9. Recomputing $\bar{\mathcal{Q}}_K$ and taking the rank gives

$$\mathrm{rank}\,(\bar{\mathcal{Q}}_K) = 9 \tag{51}$$

which is full rank. This indicates that $\mathbf{x}_{\mathrm{POI}}$, $\mathbf{b}_{\mathrm{ATT}}$, and $\mathbf{b}_{\mathrm{GIM}}$ are all observable, but $\mathbf{b}_{\mathrm{NAV}}$ is not. Intuitively, this implies that navigation biases are translated directly into POI biases. It is noted that the observability of UAV navigation biases was explored in [28], where the navigation biases were modeled as

$$\mathbf{b}_{k+1,\mathrm{NAV}} = a\mathbf{b}_{k,\mathrm{NAV}} + \mathbf{w}_{k,\mathrm{NAV}} \tag{52}$$

It was then shown that position biases are unobservable with $a = 1$, which is the bias model used here. However, if the biases are taken as autocorrelated errors, with $a \neq 1$, then the position biases are observable. However, the time scale for GPS-based navigation errors is too large to be useful here, as geolocation is desired in less than an orbit, and this would require multiple orbits.

Since the ATT and GIM states are observable, one can check the degree of observability as described in Sec. IV. First, invert $\bar{\mathcal{Q}}_K$ to get $\bar{\mathcal{P}}_K$ and then analyze the eigenvectors and eigenvalues of the submatrix of $\bar{\mathcal{P}}_K$ corresponding to $\mathbf{b}_{\mathrm{ATT}}$ and $\mathbf{b}_{\mathrm{GIM}}$. In this case, the eigenvectors and eigenvalues are

$$V = \begin{bmatrix} 0.18 & 0.68 & 0.01 & 0.04 & -0.71 & -0.01 \\ 0.01 & 0.04 & -0.47 & -0.83 & -0.01 & -0.30 \\ 0.02 & 0.00 & -0.81 & 0.28 & 0.00 & 0.51 \\ 0.70 & -0.18 & 0.24 & -0.34 & -0.02 & 0.55 \\ -0.19 & -0.68 & -0.02 & -0.01 & -0.71 & -0.01 \\ -0.66 & 0.19 & 0.24 & -0.35 & -0.01 & 0.59 \end{bmatrix} \begin{matrix} \leftarrow \text{roll} \\ \leftarrow \text{pitch} \\ \leftarrow \text{yaw} \\ \leftarrow \text{pan} \\ \leftarrow \text{tilt} \\ \leftarrow \text{scan} \end{matrix} \tag{53}$$

$$\Lambda = [\,26.45 \quad 7.56 \quad 1.55 \quad 0.64 \quad 0.00 \quad 0.00\,] \tag{54}$$

where the columns of V are the eigenvectors and the elements of Λ are the corresponding eigenvalues.

Since $\mathbf{b}_{\mathrm{ATT}}$ and $\mathbf{b}_{\mathrm{GIM}}$ have the same units, the scaled eigenvalues in Eq. (54) provide a meaningful measure of the observability, and the eigenvectors in Eq. (53) give the modes of observability. Note that large eigenvalues correspond to poor observability. The least observable mode is the combination of camera pan and camera scan, with an eigenvalue of 26.4. This indicates that a pan bias is difficult to distinguish from a scan bias. The other poorly observable mode is the combination of UAV roll and camera tilt, with an eigenvalue of 7.5. So even though, as indicated by the rank condition, all of the attitude biases are observable in a POI-centered orbit, some of them are poorly observable.

The poor observability of the combination of both ATT and GIM biases in a POI-centered orbit indicates that estimating only a subset of the biases may be effective at improving geolocation accuracy. To test this, four choices of biases to estimate are evaluated here using the 2007 flight-test data with a single UAV in a POI-centered orbit ($\Delta = 0$) about a stationary POI: no bias, GIM, ATT, and ATT-GIM. The geolocation errors for each of the four bias choices are shown in Fig. 3 for the first 5 min of the 2007 flight-test data.

Two significant observations can be made from Fig. 3. First, all forms of sensor bias estimation improve geolocation accuracy, in terms of both steady-state estimate error and convergence time. When the sensor biases are not modeled, the geolocation estimate oscillates with a period that is the same as the orbit of the UAV. When estimating the sensor bias, the geolocation estimate converges to within 1 of the POI location in 30 s, compared with more than 6 min with no bias estimation. The second important observation is that the choice of sensor biases to model has little impact on geolocation accuracy in this case: i.e., a centered orbit about a stationary POI.

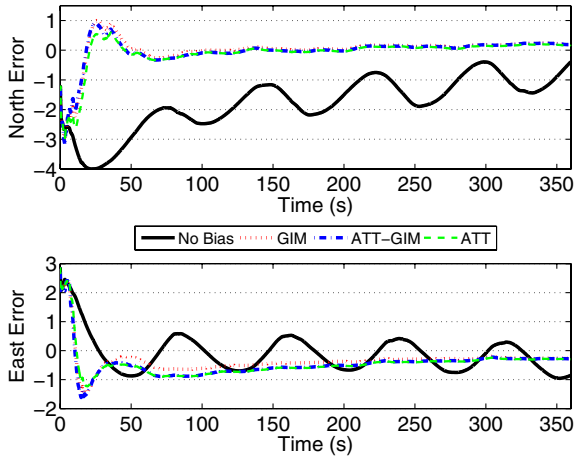

Fig. 3 Geolocation error during the first 6 min of the 2007 flight-test data with the UAV in a POI-centered orbit about a stationary POI and using four different choices of biases to estimate (no bias, GIM, ATT, and ATT-GIM).

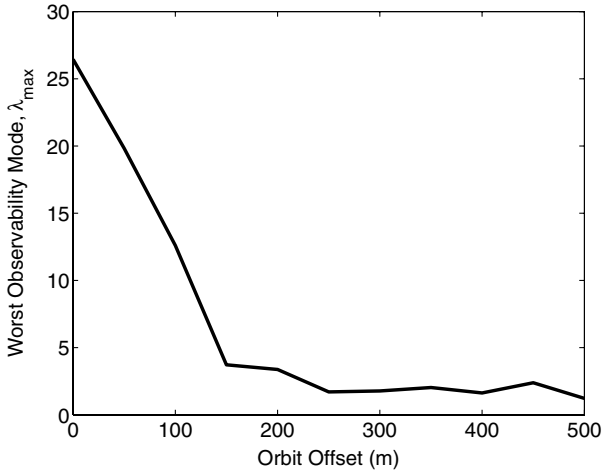

Fig. 5 Observability of least observable mode over a range of orbit offsets.

This is because the UAV attitude and camera attitude biases are poorly observable when flying in a POI-centered orbit.

As further evidence of the lack of observability in POI-centered orbits, Fig. 4 shows the estimates of the sensor biases for three bias estimation choices: GIM, ATT, and ATT-GIM. Note that the estimates for biases that are not part of that estimator are plotted as zero: e.g., the roll bias estimate for GIM bias estimation in Fig. 4b.

Consider first the camera tilt and UAV roll bias estimates, shown in Fig. 4. For a POI-centered orbit, the camera is perpendicular to the fuselage of the UAV, creating a situation in which a bias in camera tilt has the same effect as a bias in UAV roll. Consequently, the tilt bias estimate from GIM bias estimation is the same as the roll estimate from ATT bias estimation: i.e., a value of ≈ -1. Further, in the case of ATT-GIM bias estimation, the tilt bias estimate drifts positive, while the roll bias estimate drifts negative. This drift is due to the poor observability between the camera tilt and UAV roll, as described earlier and shown in Eq. (53). Interestingly, when the tilt bias estimate and the roll bias estimate are added for the ATT-GIM case, a value of ≈ -1 results, which is the same as the GIM and ATT cases. This is easiest to see near $\approx$160 s, where the circles show the convergence of all three bias estimation cases. Similar observations can be made by comparing the estimates of the other bias variables, albeit with more complicated analysis.

The lack of observability for POI-centered orbits is not necessarily a problem; in fact, it can be exploited as a benefit. If the biases are being estimated only to improve geolocation, i.e., the true biases are not required, then the reduced parameterization of the ATT *or* GIM cases will suffice to improve geolocation, as shown in Fig. 3. This also serves to reduce computation, which scales with the cube of the dimension of the state to estimated.

It is insightful to study the observability and performance of geolocation for noncentered orbits about a stationary POI. The effect of orbit offset on observability can be evaluated by considering the worst observability mode and its change with orbit offset, Δ, where the worst mode is defined to be $\lambda_{\max}$ with

$$\lambda_{\max} = \max_i \lambda_i \tag{55}$$

where λ_i are the eigenvalues of $\bar{\mathcal{P}}_K = \bar{\mathcal{Q}}_K^{-1}$. HIL simulation tests were run for orbit offsets up to $\Delta = 500$ m (equal to the orbit radius), and Fig. 5 plots $\lambda_{\max}$ as a function of the orbit offset when estimating both ATT and GIM biases. Figure 5 shows that observability significantly improves with orbit offset up to an offset of 150 m, with limited improvement afterward. These results indicate that the biases in both the UAV attitude and camera attitude can be effectively estimated with a circular orbit that has a center offset from the POI: i.e., $\Delta \neq 0$.

The effect of orbit offset on geolocation accuracy is also evaluated with HIL simulation. Thirty minutes of simulated data from the HIL simulation are used for each of the 11 orbit offsets tested: $\Delta \in [0, 0, \ldots, 500$ m$]$. Figure 6 shows the steady-state geolocation error for each of the orbit offset tests. The steady-state geolocation error is defined here to be the Euclidean distance between the POI estimate and the true POI location, averaged over the last 2 min of the 30 min of data.

Figure 6 shows that geolocation accuracy degrades with orbit offset not only for the no-bias case, but also for the GIM only and ATT only cases. This is because, as the orbit offset increases, all of the

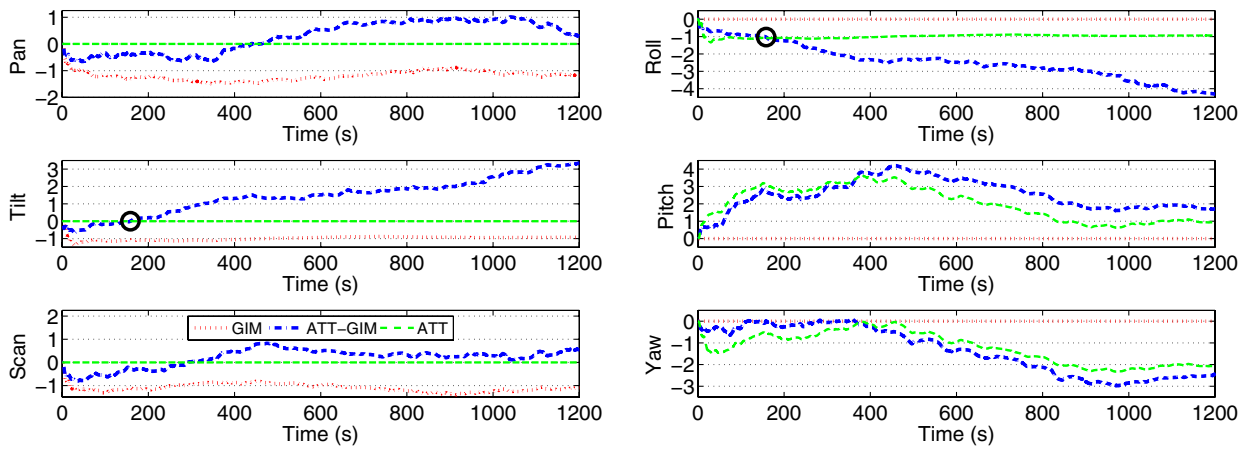

a) Camera gimbal bias estimates **b) UAV attitude bias estimates**

Fig. 4 Bias estimates for the 2007 flight-test data using a single UAV and a centered orbit around a stationary POI.

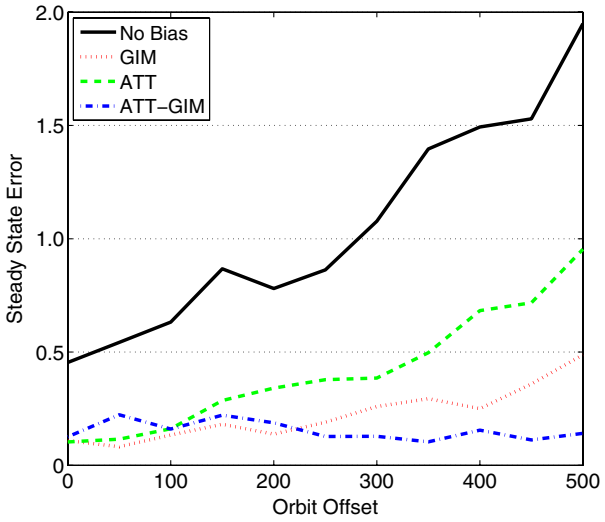

Fig. 6 Average steady-state geolocation error from HIL simulation with orbit offsets ranging from 0 to 500 m (the orbit radius was 500 m).

biases are observable, and geolocation is now dependent on all of the biases. For the ATT and GIM cases, the estimator attempts to fit an underparameterized set of biases to the true set of six. Since ATT-GIM bias estimation includes all of the biases, it is invariant to orbit offset.

2. *Cooperative UAV Flight-Test Results*

Cooperative geolocation is experimentally evaluated using the 2007 flight-test data, which included two UAVs in a circular orbit centered over a stationary POI. The experimental flight data are broken into four subsets of 6 min each. Figure 7 shows geolocation errors averaged over those four subsets. Six different cases are included in Fig. 7 based on a 3×2 selection of three cooperation choices (a single UAV, centralized with two UAVs, and decentralized with two UAVs) and two bias choices (no bias and ATT-GIM bias). The error is defined to be the Euclidean distance between the true and estimated POI locations.

Four important conclusions can be drawn from Fig. 7. First, comparing a single UAV with and without bias estimation shows that geolocation accuracy improves by approximately 75% with bias estimation. Second, comparing the decentralized no-bias vs ATT-GIM cases, bias estimation improves the convergence time ($\approx$1 min with bias estimation compared with $\approx$4 min without bias estimation), but gives approximately the same steady-state error. The centralized (no bias vs ATT-GIM) comparison gives similar results. Third, comparing a single UAV with no bias estimation with using two UAVs (decentralized or centralized) with no bias estimation shows that using two UAVs improves geolocation accuracy significantly, in terms of both the steady-state error ($\approx$1.5 for one UAV compared with $\approx$0.3 for two UAVs) and convergence time ($\approx$6 min for one UAV and $\approx$4 min for two UAVs). Fourth, with ATT-GIM bias estimation, comparing the decentralized bias estimation approach and the centralized bias estimation approach shows that the decentralized approach remains within 0.03% of the centralized approach at all times when locating a stationary POI. This shows that the algorithmic assumption in the decentralized approach, which is that the cross correlation between the biases on each of the UAVs is small and can be removed through marginalization, is reasonable in this case.

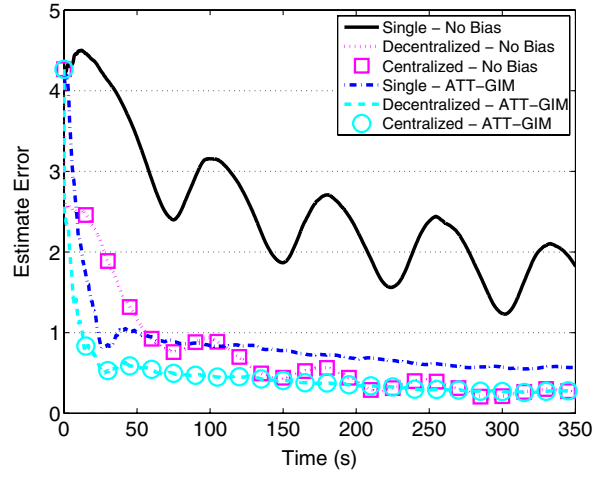

Fig. 7 Geolocation error averaged over four subsets of the 2007 flight test with three choices of cooperation (single UAV, decentralized, and centralized) and with two choices of biases to estimate (no bias and ATT-GIM bias).

C. Moving Point of Interest

Bias estimation for a moving POI is evaluated in this section using the HIL simulation data for two ScanEagle UAVs locating a moving POI, described in Sec. V.A. The path of the moving POI is based on a city driving model characterized by frequent stops and 90° turns. A representative moving-POI trajectory is shown in Fig. 8. SPOI, computed camera line-of-sight intersections with the ground, are also included in Fig. 8 as dots for reference as an approximate evaluation of the camera measurement.

A simple ballistic model is used as the POI dynamics model for the geolocation estimator and is written as

$$\mathbf{x}_{k+1,\mathrm{POI}} = \begin{bmatrix} \mathcal{I}_{3,3} & \delta t \mathcal{I}_{3,3} \\ \mathbf{0}_{3,3} & \mathcal{I}_{3,3} \end{bmatrix} \mathbf{x}_{k,\mathrm{POI}} + \begin{bmatrix} \mathbf{0}_{3,3} \\ \mathcal{I}_{3,3} \end{bmatrix} \mathbf{w}_{k,\mathrm{POI}} \tag{56}$$

where $\mathcal{I}_{3,3}$ is a 3×3 identity matrix. The POI state stacks three position states and three velocity states, both in the local NED frame.

Figure 8 also shows the estimates of the POI using one UAV for two cases of bias estimation: no bias estimation and ATT-GIM bias estimation. When no biases are estimated (solid line in Fig. 8) the estimate approximately follows the SPOI. This is due to the freedom in a ballistic POI model used here, as the estimator considers the SPOI to be a statistically reasonable estimate for the POI state. When biases are assumed in both the ATT-GIM states (dashed–dotted line), the estimate follows the true POI path more closely.

The geolocation performance (average error) for the moving-POI case is presented in Fig. 9 for a 3×2 selection of three cooperation cases (a single UAV, centralized with two UAVs, and decentralized

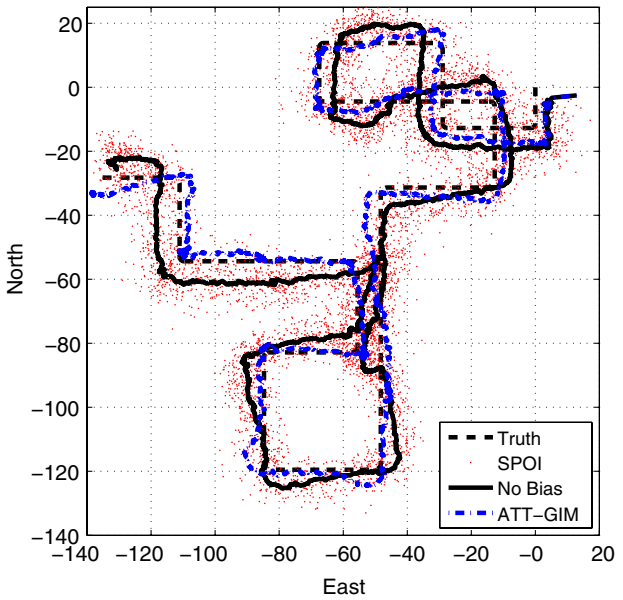

Fig. 8 Representative trajectory from the HIL city driving simulator and geolocation estimates using a single UAV and two bias estimation choices (no bias and ATT-GIM bias).

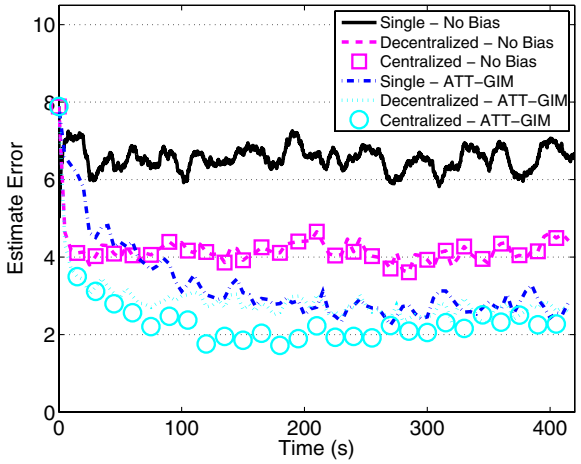

Fig. 9 Geolocation error averaged over four subsets of the HIL moving-POI test set with three choices of cooperation: single UAV, decentralized, and centralized and also with two choices of biases to estimate: no bias and ATT-GIM bias.

with two UAVs) and two bias cases (no bias and ATT-GIM bias). The data from the seven 30 min HIL tests of a moving POI are each broken into four nonoverlapping subsets of 7 min each, giving 28 data sets (seven tests varying relative phase $\beta \in [0, 30, \ldots, 180°]$ and four subsets of each). The geolocation error in Fig. 9 is the average over these 28 data sets. The average geolocation error is computed by finding the Euclidean distance from the estimated POI location and the true POI location at each time step, for each data set, and then taking the average over the 28 data sets.

Four conclusions can be drawn from Fig. 9. First, using only one UAV and not estimating biases is the least accurate approach, with a steady-state error of ≈6.5, and is used here as a baseline for comparison. Second, adding a second cooperating UAV with no bias estimation (centralized and decentralized are the same in this case) provides some reduction in steady-state error over the case with a single UAV with no bias estimation, with a steady-state error of ≈4.2. Third, including bias estimation with a single UAV provides even more improvement in steady-state error over the single-UAV no-bias case, with a steady-state error of ≈3. Fourth, the centralized and decentralized approaches for two UAVs with ATT-GIM bias estimation are the most accurate, particularly early (first 4 min) and only moderately so afterward. Finally, the decentralized approach has approximately 5% larger steady-state error than the centralized approach; this error was 0.3% in the stationary-POI case. This indicates that the moving-POI case results in a larger coupling of the biases of each UAV than does the stationary-POI case, and a small amount of information is lost through the marginalization process. This small loss of accuracy is traded with the scalability of the decentralized implementation in terms of reduced computation and communication.

VI. Conclusions

The cooperative geolocation of a point of interest (POI) using multiple UAVs with articulating camera sensors is addressed, where there are non-zero-mean errors (biases) in the estimate of the UAV state. A decentralized joint POI and bias estimation approach is proposed that uses a marginalization step allowing each UAV to model only the POI state and the local biases. Marginalization is used to share information only related to the POI state by assuming that the cross correlation between the biases across each of the UAVs is small and can be ignored. The proposed decentralized solution is scalable, in that only information about the POI is shared among the UAVs.

An observability analysis of the joint geolocation and bias estimation problem showed that biases in the UAV navigation solution are not observable, and they pass directly to the POI estimate. Biases in the UAV attitude and camera attitude are also observable, albeit poorly for the case of a single UAV in a POI-centered orbit. While potentially problematic, this poor observability of the biases allows for computational savings for the POI-centered-orbit case, by estimating only a subset of the biases without a degradation of geolocation accuracy. As the orbit center is offset from the POI, the biases are well observable. In this case, all biases must be estimated in order to yield accurate geolocation estimates; estimating only a subset of the biases degrades geolocation accuracy.

The proposed decentralized joint POI and bias estimation approach is validated using both experimental flight-test data and hardware-in-the-loop simulation data for two ScanEagle UAVs locating stationary and moving POI. Including bias estimation coupled with POI estimation improves geolocation accuracy, in terms of convergence time and steady-state estimate error, for all cases. For the single-UAV case, the steady-state estimate error is reduced by more than 50%. When locating a stationary POI, the decentralized approach recovers the centralized solution to within 0.03%. This validates the assumption that the cross correlation of the biases is small in this case. When locating a moving POI, however, the decentralized approach deviates from the centralized approach by approximately 5%. However, the small reduction in accuracy is traded for scalability in reduced computation and communication.

Appendix: Camera Measurement

The sensor measurement is formally defined as the location of the POI in the camera screen, as determined by the onboard vision system, and is given by (dropping the superscript and subscript that denote which UAV at which time step, respectively)

$$\begin{aligned}\mathbf{z} &= \mathbf{h}_{\mathrm{SCR}}(\mathbf{x}_{\mathrm{POI}}, \boldsymbol{\psi}, \mathbf{v}) \\ &= \begin{bmatrix} \lambda_y & 0 \\ 0 & \lambda_z \end{bmatrix} \begin{bmatrix} R^{\mathrm{CAM}}_{\mathrm{NED}}(2) \\ R^{\mathrm{CAM}}_{\mathrm{NED}}(3) \end{bmatrix} \left[R^{\mathrm{CAM}}_{\mathrm{NED}}(1)(\mathbf{x}_{\mathrm{POI}} - \boldsymbol{\psi}_{\mathrm{NAV}}) \right]^{-1} \\ &\times (\mathbf{x}_{\mathrm{POI}} - \boldsymbol{\psi}_{\mathrm{NAV}}) + \mathbf{v} \end{aligned} \tag{A1}$$

where $\mathbf{v}$ is the noise in the vision system and

$$\lambda_y = \frac{\tan(\mathrm{FOV}/2)}{p_{\max_y}}, \qquad \lambda_z = \frac{\tan(\mathrm{FOV}/2)}{p_{\max_z}}$$

are pixel length-scale factors, which depend on the camera field of view (FOV) and $p_{\max_{(y,z)}}$, which is the maximum camera pixels in the y and z directions. Note that the UAV position and POI location are assumed to be in a local NED frame. The rotation matrix $R^{\mathrm{CAM}}_{\mathrm{NED}}$ is a combination of the rotation matrices from the local NED frame to the aircraft body (ABC) frame and then to the camera (CAM) frame, given as

$$R^{\mathrm{CAM}}_{\mathrm{NED}} = \begin{bmatrix} R^{\mathrm{CAM}}_{\mathrm{NED}}(1) \\ R^{\mathrm{CAM}}_{\mathrm{NED}}(2) \\ R^{\mathrm{CAM}}_{\mathrm{NED}}(3) \end{bmatrix} = R^{\mathrm{CAM}}_{\mathrm{ABC}} R^{\mathrm{ABC}}_{\mathrm{NED}} \tag{A2}$$

where

$$R^{\mathrm{ABC}}_{\mathrm{NED}} = \begin{bmatrix} 1 & 0 & 0 \\ 0 & C(\phi) & S(\phi) \\ 0 & -S(\phi) & C(\phi) \end{bmatrix} \begin{bmatrix} C(\theta) & 0 & -S(\theta) \\ 0 & 1 & 0 \\ S(\theta) & 0 & C(\theta) \end{bmatrix} \begin{bmatrix} C(\psi) & S(\psi) & 0 \\ -S(\psi) & C(\psi) & 0 \\ 0 & 0 & 1 \end{bmatrix} \tag{A3}$$

$$R^{\mathrm{CAM}}_{\mathrm{ABC}} = \begin{bmatrix} C(s) & S(s) & 0 \\ -S(s) & C(s) & 0 \\ 0 & 0 & 1 \end{bmatrix} \begin{bmatrix} C(t) & 0 & S(t) \\ 0 & 1 & 0 \\ -S(t) & 0 & C(t) \end{bmatrix} \begin{bmatrix} C(p) & S(p) & 0 \\ -S(p) & C(p) & 0 \\ 0 & 0 & 1 \end{bmatrix} \tag{A4}$$

$\boldsymbol{\psi}_{\mathrm{ATT}} = [\phi, \theta, \psi]^T$ are the roll, pitch, and yaw angles of the aircraft; $\boldsymbol{\psi}_{\mathrm{GIM}} = [p, t, s]^T$ are the pan, tilt, and scan of the gimbal; and $C(\cdot)$ and $S(\cdot)$ represent $\cos(\cdot)$ and $\sin(\cdot)$, respectively.

Acknowledgments

This work was supported by the U.S. Air Force Office of Scientific Research (AFOSR) Small Business Technology Transfer program (FA9550-04-C-0072), with the In Situ Group as the lead industry organization, with Matt Wheeler as Principal Investigator. The authors wish to thank Nisar Ahmed for helpful discussions on marginalization and Mark Psiaki for helpful discussions on nonlinear observability. Sharon Heise is the AFOSR Program Manager, and Corey Schumacher from the U.S. Air Force Research Laboratory Wright-Patterson Air Force Base is the Contract Monitor.

References

[1] Furukawa, T., Bourgault, F., and Lavis, Benjamin, D.-W. H., "Recursive Bayesian Search-and-Tracking Using Coordinated UAVs for Lost Targets," *Proceedings of the IEEE International Conference on Robotics and Automation*, Inst. of Electrical and Electronics Engineers, Piscataway, NJ, May 2006.
doi:10.1109/ROBOT.2006.164208

[2] Srinivasan, S., Latchman, H., Shea, J., Wong, T., and McNair, J., "Airborne Traffic Surveillance Systems: Video Surveillance of Highway Traffic," *2nd ACM International Workshop on Video Surveillance and Sensor Networks*, New York, Oct. 2004.
doi:10.1145/1026799.1026821

[3] Hsiao, F. B., Chieri, Y.-H., Liu, T.-L., Lee, M. T., Chang, W.-Y., Han, S. Y., and Wang, Y.-H., "A Novel Uninhabited Aerial Vehicle System with Autonomous Flight and Auto-Lockup Capability," AIAA Aerospace Sciences Meeting and Exhibit, AIAA Paper 2005-1050, 2005.

[4] Jakobsen, O. C., and Johnson, E. N., "Control Architecture for a UAV Mounted Pan/Tilt/Roll Camera Gimbal," Infotech@Aerospace, AIAA Paper 2005-7145, 2005.

[5] Quigley, M., Goodrich, M., Griffiths, S., Eldredge, A., and Beard, R. W., "Target Acquisition, Localization, and Surveillance Using a Fixed-Wing Mini-UAV and Gimbaled Camera," *Proceedings of the IEEE International Conference on Robotics and Automation*, Inst. of Electrical and Electronics Engineers, Piscataway, NJ, Apr. 2005, pp. 2600–2605.

[6] Wang, I. H., Dobrokhodov, V. N., Kaminer, I. I., and Jones, K. D., "On Vision-Based Target Tracking and Range Estimation for Small UAVs," *AIAA Guidance Navigation and Control Conference*, AIAA Paper 2005-6401, San Francisco, Aug. 2005.

[7] Campbell, M. E., and Wheeler, M., "A Vision Based Geolocation Tracking System for UAVs," *Journal of Guidance, Control, and Dynamics*, Vol. 33, No. 2, 2010, pp. 521–532; also AIAA Paper 2006-6246, Keystone, CO, Aug. 2006.
doi:10.2514/1.44013

[8] Campbell, M. E., and Whitacre, W. W., "Cooperative Tracking Using Vision Measurments on SeaScan UAVs," *IEEE Transactions on Control Systems Technology*, Vol. 15, No. 4, July 2007, pp. 613–626.
doi:10.1109/TCST.2007.899177

[9] Whitacre, W., Campbell, M., Wheeler, M., and Stevenson, D., "Flight Results from Tracking Ground Targets Using SeaScan UAVs with Gimballing Cameras," *Proceedings of the American Control Conference*, Inst. of Electrical and Electronics Engineers, Piscataway, NJ, July 2007.
doi:10.1109/ACC.2007.4282696

[10] Friedland, B., "Treatment of Bias in Recursive Filtering," *IEEE Transactions on Automatic Control*, Vol. 14, No. 4, Aug. 1969, pp. 359–367.
doi:10.1109/TAC.1969.1099223

[11] Kastella, K., Yeary, B., Zadra, T., Brouillard, R., and Frangione, E., "Bias Modeling and Estimation for GMTI Applications," *International Conference on Information Fusion*, Vol. 1, July 2000.

[12] Shea, P., Zadra, T., Klamer, D., Frangione, E., and Brouillard, R., "Precision Tracking of Ground Targets," *Proceedings of the IEEE Aerospace Conference*, Vol. 3, March 2000, pp. 473–482.
doi:10.1109/AERO.2000.879873

[13] Lin, X., Bar-Shalom, Y., and Kirubarajan, T., "Multisensor Multitarget Bias Estimation for General Asynchronous Sensors," *IEEE Transactions on Aerospace and Electronic Systems*, Vol. 41, No. 3, July 2005, pp. 899–921.
doi:10.1109/TAES.2005.1541438

[14] Okello, N., and Challa, S., "Joint Sensor Registration and Track to Track Fusion for Distributed Trackers," *IEEE Transactions on Aerospace and Electronic Systems*, Vol. 40, No. 3, July 2004, pp. 808–823.
doi:10.1109/TAES.2004.1337456

[15] Dogancay, K., "Bias Compensation for Bearings-Only Pseudolinear Target Track Estimator," *IEEE Transactions on Signal Processing*, Vol. 54, No. 1, Jan. 2006, pp. 59–68.
doi:10.1109/TSP.2005.861088

[16] Durrant-Whyte, H., and Stevens, M., "Data Fusion in Decentralized Sensing Networks," *The 4th International Conference on Information Fusion*, Montreal, Canada, 2001.

[17] Sukkarieh, S., Nettleton, E., Kim, J.-H., Ridley, M., Goktogan, A., and Durrant-Whyte, H., "The ANSER Project: Data Fusion Across Multiple Uninhabited Air Vehicles," *International Journal of Robotics Research*, Vol. 22, No. 7-8, July–Aug. 2003, pp. 505–539.
doi:10.1177/02783649030227005

[18] Rao, B. S. Y., Durrant-Whyte, H. F., and Sheen, J. A., "A Fully Decentralized Multi-Sensor System for Tracking and Surveillance," *International Journal of Robotics Research*, Vol. 12, No. 1, Feb. 1993, pp. 20–44.
doi:10.1177/027836499301200102

[19] Mutambara, A. G. O., "Information Based Estimation for Both Linear and Nonlinear Systems," *Proceedings of the American Control Conference*, Inst. of Electrical and Electronics Engineers, Piscataway, NJ, 1999.
doi:10.1109/ACC.1999.783583

[20] Miller, I., and Campbell, M., "Particle Filtering for Map-Aided Localization in Sparse GPS Environments," *IEEE Conference on Robotics and Automation*, Inst. of Electrical and Electronics Engineers, Piscataway, NJ, May 2008.
doi:10.1109/ROBOT.2008.4543474

[21] Whitacre, W., and Campbell, M., "Cooperative Geolocation with UAVs Under Communication Constraints," *AIAA Guidance Navigation and Control Conference*, AIAA Paper 2007-6759, Hilton Head, SC, Aug. 2007.

[22] Bryson, A. E., and Johansen, D. E., "Linear Filtering for Time-Varying Systems Using Measurements Containing Colored Noise," *IEEE Transactions on Automatic Control*, Vol. 10, No. 1, Jan. 1965, pp. 4–10.
doi:10.1109/TAC.1965.1098063

[23] Psiaki, M. L., "Autonomous Low-Earth-Orbit Determination from Magnetometer and Sun Sensor Data," *Journal of Guidance, Control, and Dynamics*, Vol. 22, No. 2, March–April 1999, pp. 296–304.
doi:10.2514/2.4378

[24] Psiaki, M. L., "Autonomous Low-Earth-Orbit Determination for Two spacecraft from Relative Position Measurements," *Journal of Guidance, Control, and Dynamics*, Vol. 22, No. 2, March–April 1999, pp. 305–312.
doi:10.2514/2.4379

[25] Stevenson, D., Wheeler, M., Campbell, M., Whitacre, W., Rysdyk, R., and Wise, R., "Cooperative Tracking Flight Test," AIAA Guidance Navigation and Control Conference, AIAA Paper 2007-6756, Hilton Head, SC, Aug. 2007.

[26] Stevenson, D., Wheeler, M., Matlack, C., Wise, R., and Whitacre, W., "Developing a Robust and Flexible Simulation Environment to Support Cooperative Tracking of UAVs," AIAA Paper 2007-6565, Aug. 2007.

[27] Wise, R., and Rysdyk, R., "UAV Coordination for Autonomous Target Tracking," AIAA Guidance Navigation and Control Conference, AIAA Paper 2006-6453, Keystone, CO, Aug. 2006.

[28] Bar-Shalom, Y., "Mobile Radar Bias Estimation Using Unknown Location Targets," *International Conference on Information Fusion*, Vol. 1, Paris, July 2000.